J|A|C|S
ARTICLES

Published on Web 10/23/2008

Antenna Chemistry with Metallic Single-Walled Carbon Nanotubes

Juan G. Duque,[†] Matteo Pasquali,[*,†,‡] and Howard K. Schmidt[*,†]

Department of Chemical and Biomolecular Engineering and Department of Chemistry, The Smalley Institute for Nanoscale Science & Technology, Rice University, 6100 South Main, Houston, Texas 77005

Received May 3, 2008; E-mail: hks@rice.edu; mp@rice.edu

Abstract: We show that, when subjected to microwave fields, surfactant-stabilized single-walled carbon nanotubes (SWNTs) develop polarization potentials at their extremities that readily drive electrochemical reactions. In the presence of transition metal salts with high oxidation potential (e.g., $FeCl_3$), SWNTs drive reductive condensation to metallic nanoparticles with essentially diffusion-limited kinetics in a laboratory microwave reactor. Using $HAuCl_4$, metallic particles and sheaths deposit regioselectively at the SWNT tips, yielding novel SWNT−metal composite nanostructures. This process is shown to activate exclusively metallic SWNTs; a degree of diameter selectivity is observed using acceptors with different oxidation potentials. The reaction mechanism is shown to involve Fowler−Nordheim field emission in solution, where electric fields concentrate at the SWNT tips (attaining $\sim 10^9$ V/m) due to the SWNT high aspect ratio ($\sim$1000) and gradient compression in the insulating surfactant monolayer. Nanotube antenna chemistry is remarkably simple and should be useful in SWNT separation and fractionation processes, while the unusual nanostructures produced could impact nanomedicine, energy harvesting, and synthetic applications.

Introduction

Single-wall carbon nanotubes (SWNTs) comprise a large family of cylindrical all-carbon polymers with remarkable mechanical and electrical properties; the specific structure of individual SWNT can be uniquely described by an (n, m) vector (type) that defines its diameter and chirality.[1] Roughly two-thirds of SWNT species are direct band gap semiconductors that fluoresce in the near-infrared.[2] About two percent are ‘true’ metals with a finite density of states at the Fermi level, while the rest are semimetals. Individual metallic SWNT are essentially ballistic conductors that support DC current densities approaching 10^9 A/cm^2.[3] As a consequence, metallic SWNTs have a high axial dielectric constant[4] and rapidly polarize in response to externally applied electric fields, with expected axial resonance in the THz regime.[5] Therefore, metallic SWNTs can be considered nanoscale antennae, and this polarization-based ‘antenna effect’ has several interesting and useful manifestations. For example, radio frequency (RF) dielectrophoresis[6] can be employed to manipulate and type-separate suspensions of individualized SWNT,[2] while SWNT networks have been shown to efficiently convert electromagnetic radiation into heat across the RF,[7] microwave (MW),[8] and optical[9] frequency regimes. Their high aspect ratio, $\beta \equiv L/D \sim 1000$, provides a localized apparent field amplification factor (equal to the aspect ratio) at their tips, which enables substantial field emission currents in vacuo at nominal field strengths around 10^6 V/m.[10] There are a few reports of similar effects *in aqueous solution* using supported multiwall carbon nanotube electrodes in DC or quasi-static fields, including production of solvated electrons[11] and electrodeposition on the ends of bundles.[12]

Separately, spontaneous reduction−oxidation (redox) processes involving electron transfers to and from individualized SWNT in anionic surfactant suspensions[13] have become an active research topic. The UV−visible absorption peaks of semiconducting SWNT bleach selectively upon protonation in acidic media.[14] Near IR fluorescence quenching has been used

† Department of Chemical and Biomolecular Engineering.
‡ Department of Chemistry.

(1) Saito, R.; Fujita, M.; Dresselhaus, G.; Dresselhaus, M. S. *Appl. Phys. Lett.* **1992**, *60*, 2204–2206.
(2) O’Connell, M. J.; Bachilo, S. M.; Huffman, C. B.; Moore, V. C.; Strano, M. S.; Haroz, E. H.; Rialon, K. L.; Boul, P. J.; Noon, W. H.; Kittrell, C.; Ma, J. P.; Hauge, R. H.; Weisman, R. B.; Smalley, R. E. *Science* **2002**, *297*, 593–596.
(3) McEuen, P. L.; Fuhrer, M. S.; Park, H. K. *IEEE Trans. Nanotechnol.* **2002**, *1*, 78–85.
(4) Benedict, L. X.; Louie, S. G.; Cohen, M. L. *Phys. Rev. B* **1995**, *52*, 8541–8549.
(5) Hao, J.; Hanson, G. W. *IEEE Trans. Nanotechnol.* **2006**, *5*, 766–775.
(6) Krupke, R.; Hennrich, F.; von Lohneysen, H.; Kappes, M. M. *Science* **2003**, *301*, 344–347.
(7) Gannon, C. J.; Cherukuri, P.; Yakobson, B. I.; Cognet, L.; Kanzius, J. S.; Kittrell, C.; Weisman, R. B.; Pasquali, M.; Schmidt, H. K.; Smalley, R. E.; Curley, S. A. *Cancer* **2007**, *110*, 2654–2665.
(8) Imholt, T. J.; Dyke, C. A.; Hasslacher, B.; Perez, J. M.; Price, D. W.; Roberts, J. A.; Scott, J. B.; Wadhawan, A.; Ye, Z.; Tour, J. M. *Chem. Mater.* **2003**, *15*, 3969–3970.
(9) Ajayan, P. M.; Terrones, M.; de la Guardia, A.; Huc, V.; Grobert, N.; Wei, B. Q.; Lezec, H.; Ramanath, G.; Ebbesen, T. W. *Science* **2002**, *296*, 705–705.
(10) Bonard, J. M.; Salvetat, J. P.; Stockli, T.; de Heer, W. A.; Forro, L.; Chatelain, A. *Appl. Phys. Lett.* **1998**, *73*, 918–920.
(11) Krivenko, A. G.; Komarova, N. S.; Stenina, E. V.; Sviridova, L. N.; Kurmaz, V. A.; Kotkin, A. S.; Muradyan, V. E. *Russ. J. Electrochem.* **2006**, *42*, 1047–1054.
(12) Bradley, J. C.; Babu, S.; Ndungu, P. *Fullerenes Nanotubes Carbon Nanostruct.* **2005**, *13*, 227–237.
(13) Moore, V. C.; Strano, M. S.; Haroz, E. H.; Hauge, R. H.; Smalley, R. E.; Schmidt, J.; Talmon, Y. *Nano Lett.* **2003**, *3*, 1379–1382.

10.1021/ja803300u CCC: $40.75

to monitor diameter-selective oxidation of semiconducting SWNT by organic acceptors.[15] Similarly, aqueous suspensions of acid-oxidized SWNT (bearing anionic carboxylic acid groups) display selective interactions between metallic SWNT and nucleophilic (electron-rich) species like alkyl amines[16] and bromine.[17] These results are consistent with a key spectroelectrochemical Raman study that attributes diameter- and class-specific redox potential variations to systematic differences in absolute Fermi levels.[18] Representative redox reactions with transition metal species include electroless deposition of gold and platinum on SiO_2-supported SWNT,[19] glucose sensors based on SWNT fluorescence quenching by ferricyanide ion,[20] silver nanoparticle production upon illumination of DNA-wrapped SWNT,[21] and selective modification of carbon nanotubes with metal salt solution via bipolar electrochemistry.[22] Other techniques have been reported to obtain homogeneous and indiscriminate metal nanoparticle coatings around carbon nanotubes (CNTs).[23−26]

Here, we explore the intersection of SWNT redox chemistry and antenna effects and demonstrate facile redox processes initiated by microwave field-induced dipoles in well-dispersed SWNT−surfactant suspensions: nanotube antenna chemistry. We find that electric fields at microwave frequencies readily activate redox reactions preferentially with metallic SWNT. The process directly reduces transition metal ions in solution to produce nanoparticles, both free-floating and regiospecifically deposited on nanotube extremities, along with partial diameter selectivity based on the oxidation potential of the acceptor species involved. We demonstrate a charge transfer mechanism based on Fowler−Nordheim field emission. This process is quite distinct from previous reports using MW fields to simply heat multiwall carbon nanotube (MWNT) aggregates in the presence of transition metal ion mixtures, which generates disordered metal deposition on their sidewalls.[27−29] The reaction reported here yields novel composite nanostructures that could prove useful in applications as varied as RF thermoablation,[7] photothermal ablation,[30] and photoconversion.[31]

Results and Discussion

Figure 1a shows the polarized electric field structure around individual bare and surfactant-coated metallic SWNT immersed in water. The nanotubes have length $L = 1\ \mu$m and diameter $D = 1$ nm, and are fully aligned with an electric field $E = 1$ V/μm (10^6 V/m). Good conductors maintain uniform potential by redistribution of charge when subjected to external electric fields; the tubes are set at 0 V, the potential at their midpoint. The apparent electric field strength at the tip of the bare nanotube is amplified by geometric effects by about $\beta/2$, to yield $E_{tip} \approx 500$ V/μm.[32] The local field strength decays rapidly with distance r from the SWNT, by r^{-2} away from the hemispherical ends, and r^{-1} away from the sidewalls of the SWNT, respectively. The SDBS surfactant layer compresses further the electric field gradient around the SWNT tip, as discussed quantitatively below. In alternating (AC) fields, an induced potential of $\delta U = \pm EL/2 \approx \pm 0.5$ V is expected between the SWNT tips and the electrolyte bath a few nanometers away, significantly modulating their normal redox potential(s). Semiconducting SWNT polarize weakly and are essentially unaffected by such applied fields.[6] This model serves to visually illustrate our hypothesis that electric fields (e.g., in a microwave reactor) will interact exclusively with suspended metallic SWNT to drive electron transfer reactions, especially at their tips.

We performed a matrix of control experiments with various SWNT-surfactant suspensions and transition metal acceptor species to screen out systems with spontaneous redox reactions and isolate conditions wherein electron transfer reactions could be unambiguously attributed to electric field stimulation (see Experimental Section). One milliliter surfactant−SWNT samples (1 wt% surfactant, 10 mg/L SWNT) and 30 μL metal salt solution (1 mM) were heated to 55 °C for 2 h, then characterized with UV−visible absorbance, near IR fluorescence, and atomic force microscopy (AFM); no specific reducing agents[33] were employed. Results are summarized in Figure 1b. The nonionic surfactants Triton-X (TX) and Pluronics (F88) and the cationic surfactant cetyltrimethylammonium bromide (CTAB) supported rapid spontaneous reactions with most metal salts tested, qualitatively indicated by producing colored solutions as well as nanoparticles directly observable by AFM. No spontaneous reactions were observed in sodium dodecylbenzene sulfonate (SDBS) suspensions with any of the acceptors listed. The smaller anionic surfactant, sodium dodecyl sulfonate (SDS), supported very slow reactions (taking over 48 h) with H_2PtCl_6 or $HAuCl_4$. We also verified that no detectable (by UV−vis and AFM) nanoparticles were produced when SDBS solutions (without SWNT) were heated with the listed transition metal salts in a multimode microwave reactor ($MARS_X$, CEM, 2.54 GHz) at 1000 W for 10 s (standard MW protocol used throughout this work). MW processing increased their temperature by an average of 35.7 (±1) °C, regardless of the metal salt employed.

All further tests of MW field-induced chemistry were therefore performed with SDBS. Metal salts were reduced to metal nanoparticles in this system exclusively when activated by MW radiation. SWNT/SDBS + $HAuCl_4$ sample temperatures increased by 36.2 (±1) °C during the procedure. This negligible

(14) Strano, M. S.; Huffman, C. B.; Moore, V. C.; O'Connell, M. J.; Haroz, E. H.; Hubbard, J.; Miller, M.; Rialon, K.; Kittrell, C.; Ramesh, S.; Hauge, R. H.; Smalley, R. E. *J. Phys. Chem. B* **2003**, *107*, 6979–6985.
(15) O'Connell, M. J.; Eibergen, E. E.; Doorn, S. K. *Nat. Mater.* **2005**, *4*, 412–418.
(16) Chattopadhyay, D.; Galeska, L.; Papadimitrakopoulos, F. *J. Am. Chem. Soc.* **2003**, *125*, 3370–3375.
(17) Chen, Z. H.; Du, X.; Du, M. H.; Rancken, C. D.; Cheng, H. P.; Rinzler, A. G. *Nano Lett.* **2003**, *3*, 1245–1249.
(18) Okazaki, K.; Nakato, Y.; Murakoshi, K. *Phys. Rev. B* **2003**, *68*, 35434.
(19) Choi, H. C.; Shim, M.; Bangsaruntip, S.; Dai, H. *J. Am. Chem. Soc.* **2002**, *124*, 9058–9059.
(20) Barone, P. W.; Strano, M. S. *Angew. Chem. Int. Ed.* **2006**, *45*, 8138–8141.
(21) Zheng, M.; Rostovtsev, V. V. *J. Am. Chem. Soc.* **2006**, *128*, 7702–7703.
(22) Warakulwit, C.; Nguyen, T.; Majimel, J.; Delville, M. H.; Lapeyre, V.; Garrigue, P.; Ravaine, V.; Limtrakul, J.; Kuhn, A. *Nano Lett.* **2008**, *8*, 500–504.
(23) Liu, Y. J.; Zhang, Z. H.; Nie, L. H.; Yao, S. Z. *Electrochim. Acta* **2003**, *48*, 2823–2830.
(24) Aminur Rahman, G. M.; Guldi, D. M.; Zambon, E.; Pasquato, L.; Tagmatarchis, N.; Prato, M. *Small* **2005**, *1*, 527–530.
(25) Jiang, K.; Eitan, A.; Schadler, L. S.; Ajayan, P. M.; Siegel, R. W.; Grobert, N.; Mayne, M.; Reyes-Reyes, M.; Terrones, H.; Terrones, M. *Nano Lett.* **2003**, *3*, 275–277.
(26) Ellison, W. J. *J. Phys. Chem. Ref. Data* **2007**, *36*, 1–18.
(27) Chen, W. X.; Gui, H.; Lee, J. Y.; Liu, Z. L. *Chem. J. Chin. Univ. (Chinese)* **2003**, *24*, 2285–2287.
(28) Chen, W.-X.; Lee, J. Y.; Liu, Z. *Mater. Lett.* **2004**, *58*, 3166–3169.
(29) Luo, Y. S.; Li, S. Q.; Ren, Q. F.; Liu, J. P.; Xing, L. L.; Wang, Y.; Yu, Y.; Jia, Z. J.; Li, J. L. *Cryst. Growth Des.* **2007**, *7*, 87–92.
(30) Kam, N. W. S.; O'Connell, M.; Wisdom, J. A.; Dai, H. J. *Proc. Natl. Acad. Sci. U.S.A.* **2005**, *102*, 11600–11605.
(31) Kymakis, E.; Amaratunga, G. A. J. *Appl. Phys. Lett.* **2002**, *80*, 112–114.
(32) Buldum, A.; Lu, J. P. *Phys. Rev. Lett.* **2003**, *91*, 236801.
(33) Kim, F.; Song, J. H.; Yang, P. D. *J. Am. Chem. Soc.* **2002**, *124*, 14316–14317.

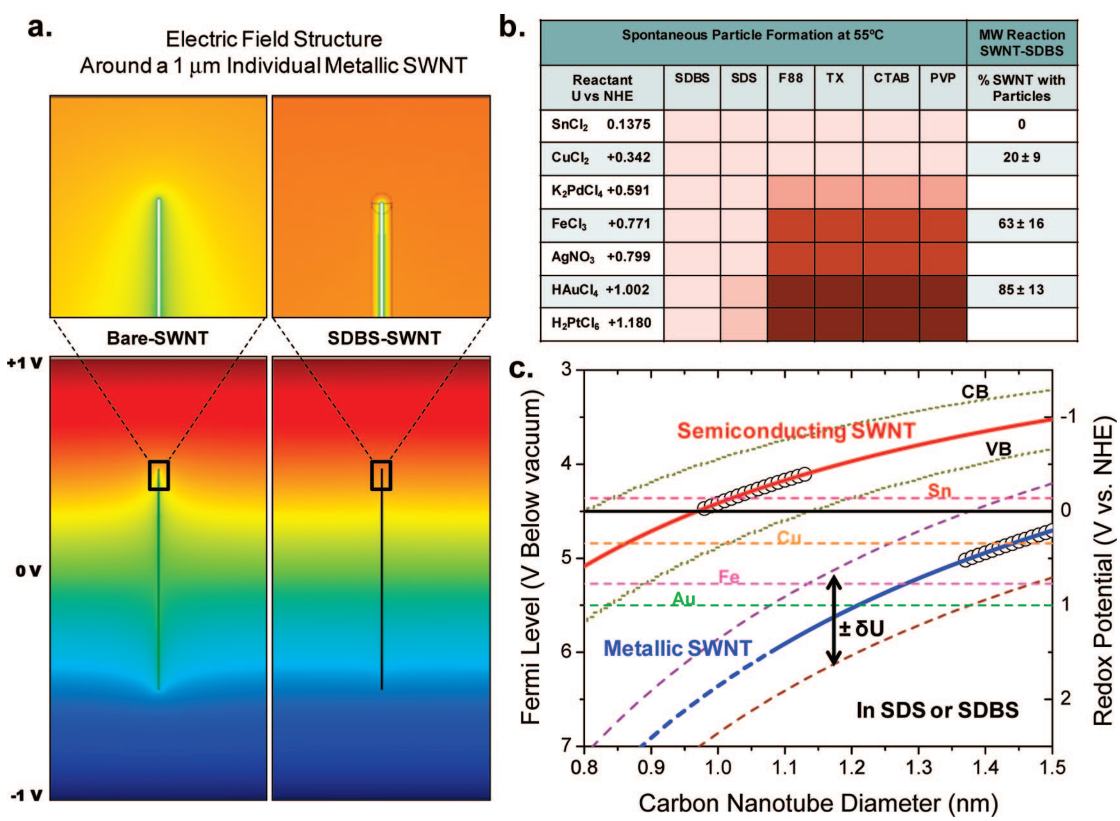

Figure 1. SWNT redox properties and electric field interactions. (a) Electric field structure around a SWNT (diameter 1 nm, length 1 μm) in a constant 1 V/μm field, with (left) and without (right) the 3 nm surfactant layer (see Supporting Information). (b) Summary of spontaneous and MW-stimulated nanoparticle formation using various combinations of metal salts and surfactants (dark = spontaneous particle formation; light = no particles). (c) Estimated SWNT redox potentials.

temperature difference eliminates the possibility of significant localized thermal effects via direct MW heating of these well-dispersed nanotubes. Particle formation in this case is plainly driven by microwave activation and not by a purely thermal process. Examination of the AFM images (discussed below) shows that while a substantial fraction of the SWNTs have attached metal particles, others are devoid of particles. The rightmost column in Figure 1b shows the percentage (std. dev.) of nanotubes with attached nanoparticles as directly observed by AFM. The duration of the experiment (10 s) is about 3 orders of magnitude higher than the characteristic times for dipolar alignment[34] and Brownian rotation[35] (few milliseconds), and the average experimental field strength of 3.5×10^5 V/m yields a dielectric alignment energy far in excess of the thermal energy kT (details in Supporting Information), indicating that metallic SWNT aligned with the field and polarized. Interestingly, the percentage of SWNT with attached nanoparticles decreases monotonically with the oxidation potential of the transition metal acceptor employed. This fraction also approximates the proportion of metallic SWNT with redox potentials more negative than the acceptor employed (see Figure 1c). The SWNT redox landscape including metallic SWNT depicted in Figure 1c is extrapolated from spectroelectrochemical Fermi level observations reported by Okazaki, et al.[18] and plotted in the manner introduced by O'Connell et al.[15] for semiconducting SWNT (see Supporting Information for details). If the MW process only activates metallic SWNT via antenna processes, then the reacting-fraction data shown here provide experimental support for the diameter dependence of the redox potential of metallic SWNT indicated in Figure 1c and further implies that the fundamental process involves transfer of electrons from metallic SWNT to acceptors with higher oxidation potential.

Figures 2a−c contrast the morphology of nanoparticles generated by spontaneous (thermal) and microwave-driven processes. AFM of a representative spontaneous reaction product, $HAuCl_4$ with SWNT suspended in F88, clearly shows a combination of free metal particles and nonselective sidewall decoration of the SWNTs (Figure 2a). This reaction mixture turned reddish and developed a strong UV−vis absorption peak at 523 nm within 10 min of warming in a water bath to 55 °C; both factors are indicative of gold nanoparticle formation.[33] In contrast, when SDBS−SWNT suspensions were irradiated in the microwave reactor for only 10 s at 1000 W in the presence of $HAuCl_4$, the solutions immediately displayed color changes and UV−vis absorbance features characteristic of Au nanoparticle formation (Figure 2d). The Au reduction produces hydrochloric acid (HCl), which accounts for the small change of pH after the reaction goes to completion.[36] Likely, the overall reaction follows the mechanism proposed by Warakulwit et al.:[22]

$$\text{(a)}\quad AuCl_4^- + 4e^- \rightarrow Au^\circ + 4Cl^-$$

$$\text{(b)}\quad 2H_2O \rightarrow O_2 + 4e^- + 4H^+$$

$$\text{(c)}\quad 4Cl^- + 4H^+ \rightarrow 4HCl$$

(34) Jones, T. B. *Electromechanics of Particles*; Cambridge University Press: NY, 1995.
(35) Duggal, R.; Pasquali, M. *Phys. Rev. Lett.* **2006**, *96*, 4. Mendes, M. J.; Schmidt, H. K.; Pasquali, M. *J. Phys. Chem. B* **2008**, *112*, 7467–7477.

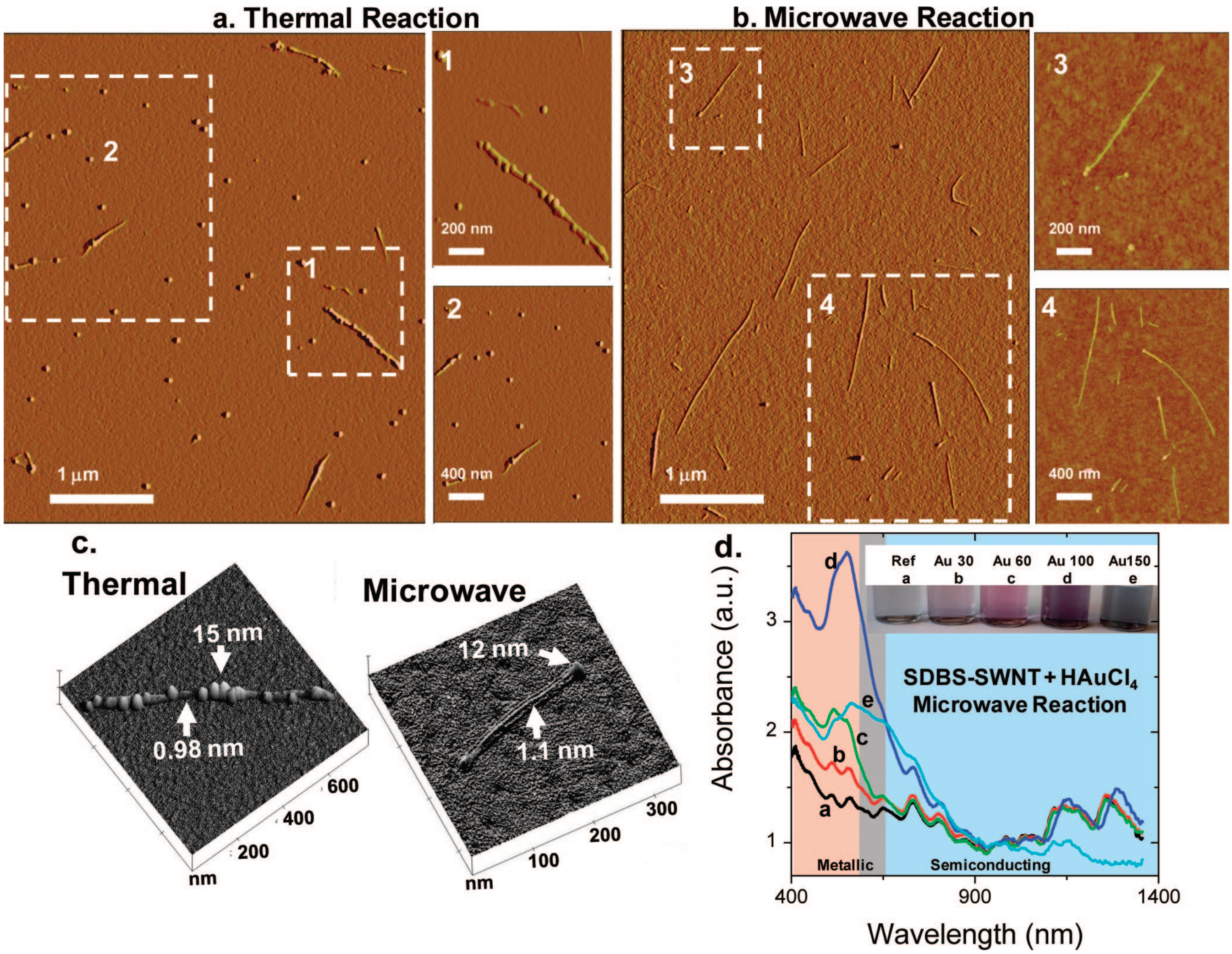

Figure 2. SWNT−Au nanoparticle morphologies. (a, b) Representative AFM images of spontaneous and indiscriminate sidewall decoration (a) and tip-selective (b) reduction of Au metal salts onto SWNTs by thermal (a) and MW (b) reduction. (c) Three-dimensional thermal and MW reduction of Au metal particles. (d) Absorbance of microwave-driven reaction of SDBS−SWNT with different amounts of 1 mM $HAuCl_4$ (0 μL reference, black; 30 μL, red; 60 μL, green; 100 μL, blue; and 150 μL, light blue).

Several factors support this reaction scheme: (a) metallic SWNTs have a substantial positive reduction potential in this system (Figure 1c), (b) modulation by the MW field will periodically induce at the SWNT tips a potential higher than their quiescent reduction potential, and (c) after electron ejection, the SWNT will be positively charged and will have even higher oxidizing power. In combination, these factors appear to generate sufficiently high potential to oxidize water and free the protons needed to balance the chloride ion and produce HCl, consistent with the observed pH shift. The amount of oxygen generated is not sufficient to generate bubbles.[22,37,38]

AFM images of SWNTs treated in this manner show a highly preferential deposition of Au nanoparticles at the tips of the SWNTs (Figure 2b.3). Raising the initial gold concentrations (150 μM Au) resulted in progressive growth of apparently coaxial metal sheaths extending back from the tips of some of the SWNTs (Figure 2b.4). These sheaths have a fairly uniform height of 10 nm, while the tip particles averaged 14 nm in height by AFM. Reactions yielding cylindrical deposits developed a purplish color and the 530 nm feature broadened significantly to the red, entirely consistent with the known spectroscopic characteristics of gold nanorods (Figure 2d,e).[33] Overall, these deposition structures almost perfectly reflect the locations of high field gradients around the SWNT tips, in good accord with our model for antenna chemistry with metallic SWNT (additional spectroscopic and microscopic evidence of tip deposition and sheath formation is available in Supporting Information). Notably, we observe the following differences with respect to ref 22: by using surfactants that amplify the effective field strength, we induce deposition with moderate MW fields instead of very high DC (10−30 kV) ones; instead of large-diameter MWNTs, we use SWNTs and demonstrate selectivity toward large-diameter (small bandgap) as well as metallic SWNTs; we obtain deposition at both ends of the SWNTs instead of only one end.[22]

To directly probe SWNT type selectivity in these reactions, we analyzed the UV−vis and *liquid-phase* Raman signatures of SDBS−SWNT−$HAuCl_4$ mixtures after MW processing and mild centrifugation (MicroD, Fisher Scientific, at 4500*g* for 10 min). This quickly removes larger Au particle-containing species from solution due to their high density; we found that similar

(36) After Au reduction the pH of the suspension decreased about 0.8 units (6.15 to 5.35). After 3 days the pH returned almost to that of the starting point (6.03).
(37) Truesdale, G. A.; Downing, A. L. *Nature* **1954**, *173*, 1236–1236.
(38) Fox, C. J. J. *Trans. Faraday Soc.* **1907**, *5*, 68–87.

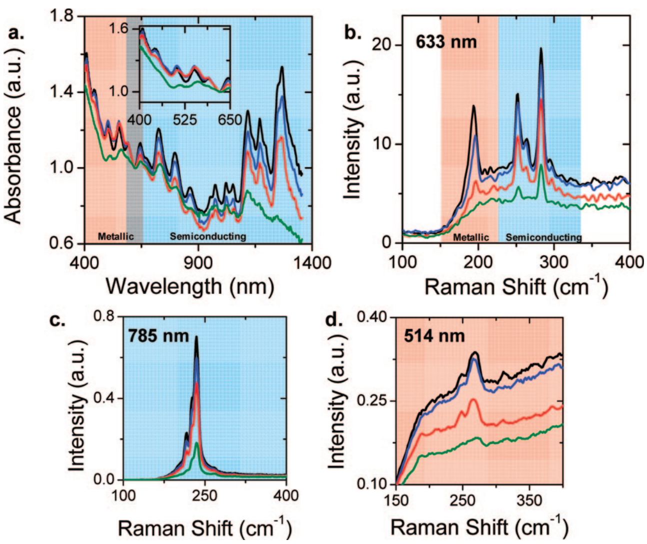

Figure 3. SWNT selectivity in MW-driven redox reactions: supernatant. (a−d) Absorbance (a) and *liquid-phase* Raman RBMs using 660 nm excitation (b), 785 nm excitation (c), and 514 nm excitation (d) spectra of SDBS−SWNT−Au suspensions after addition of different amounts of 1 mM Au salt solutions (0 μL reference, black; 100 μL, blue; 300 μL, red; and 500 μL, green) and subsequent MW processing.

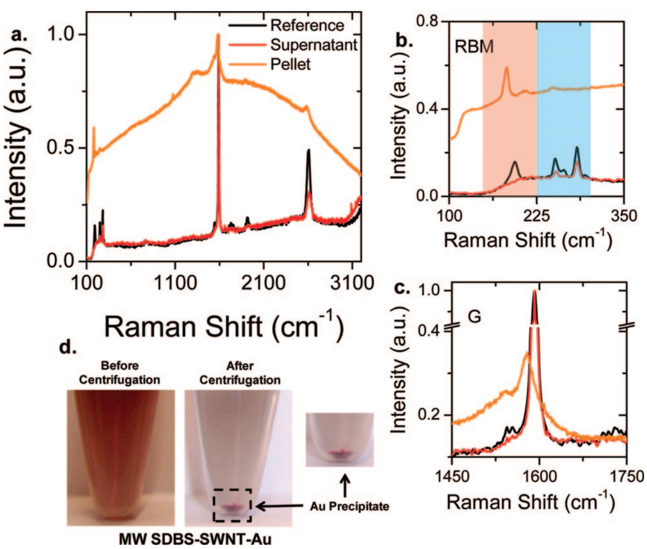

Figure 4. SWNT selectivity in MW-driven redox reactions: precipitate. (a−c) *Liquid-phase* Raman spectra using 660 nm excitation from SDBS−SWNT−Au precipitate (orange), reference (black), and supernatant (red). (b) RBM section. (c) G peak. (d) Representative image of the SDBS−SWNT−Au suspension before and after centrifugation.

results could also be obtained by letting the solution settle naturally for several days. Spectra from the supernatant after centrifugation are shown in Figure 3, while Figure 4 shows spectra obtained from resuspended pellets generated upon mild centrifugation. Figure 3a,b shows the spectral effect of adding three different amounts of 1 mM $HAuCl_4$ solution to the SWNT−SDBS suspension prior to MW processing compared to the reference suspension without gold (black trace). A significant and progressive depletion of the metallic peaks (400−650 nm) (inset, Figure 3a) is seen with increasing $HAuCl_4$ concentration, along with eventual bleaching of the E_{11} transitions for the large diameter semiconductors (1100−1400 nm). Further evidence of type selectivity in this process is provided by *liquid-phase* Raman spectra obtained using three different excitation wavelengths that are in resonance with different populations of HiPco SWNTs (514 nm, in resonance with mainly metallic tubes; 633 nm, which samples a portion of both metallic and semiconducting SWNT populations; and 785 nm, in resonance with mainly semiconducting tubes).[39−41] Importantly, *liquid-phase* Raman avoids morphology-related modifications previously noted with precipitated SWNT[42] and allows quantitative interpretation by integrating the area of radial breathing mode (RBM) peaks for metallic and semiconducting SWNT populations. Figure 3b−d show the RBM peaks of the supernatant solution using the three different excitation wavelengths (b) 633 nm, (c) 785 nm, and (d) 514 nm (see Supporting Information for additional spectra). Figure 3b shows that when the SWNT suspension is MW processed with 500 μL of $HAuCl_4$ solution, essentially all of the metallic SWNT species are apparently removed after centrifugation, yielding a supernatant highly enriched in small-diameter semiconducting SWNT. We also observed that the integrated area of the metallic SWNT peak decreases exponentially with gold concentration. To further confirm the metallic depletion and diameter (d_t) selectivity, we obtained Raman spectra using 514 nm excitation, which brings metallic SWNT in our samples into resonance (Figure 3d). We observed that after the addition of 500 μL of $HAuCl_4$ and MW processing (green trace), the RBM features associated with the metallic SWNT were depleted approximately 90% compared to the starting material (black trace). Figure 3c shows Raman spectra excited at 785 nm (sensitive to semiconducting SWNT); the shoulders at 215 and 225 cm^{-1} ((9,7), $d_t = 1.103$ nm and (10,5), $d_t = 1.050$ nm, respectively) decrease somewhat more rapidly than the main peak at 233 cm^{-1}, which is associated with the smaller (11,3) ($d_t = 1.014$ nm).[40,43] This modest effect indicates a slight preference for interactions between larger diameter semiconducting SWNT (or bundles containing them[44]) and the gold acceptor species, similar to prior reports employing organic acceptors.[15]

We also carried out MW activation experiments using CoMoCat SWNT; these have comparable length but significantly smaller average diameter[45] than HiPco SWNT (0.89 nm vs 1.1 nm, respectively), and therefore should reside at higher oxidation potentials according to the redox landscape depicted in Figure 1c. Interestingly, MW processing of SDBS-suspended CoMoCat SWNT with $HAuCl_4$ failed to generate gold nanoparticles. This could indicate that the native redox potential of the metallic SWNT strongly influences the rate of the MW reaction.

The SWNT+Au pellets generated by centrifugation were resuspended in 100 μL of DI water in order to obtain liquid-phase Raman using 633 nm excitation. The reference SWNT suspension displayed no color change after MW processing, nor was a pellet formed during centrifugation. SWNTs are present in both the supernatant and pellet, as shown by their key

(39) Kataura, H.; Kumazawa, Y.; Maniwa, Y.; Umezu, I.; Suzuki, S.; Ohtsuka, Y.; Achiba, Y. *Synth. Met.* **1999**, *103*, 2555–2558.
(40) Maultzsch, J.; Telg, H.; Reich, S.; Thomsen, C. *Phys. Rev. B* **2005**, *72*, 16.
(41) Telg, H.; Maultzsch, J.; Reich, S.; Thomsen, C. *Phys. Rev. B* **2006**, *74*, 5.
(42) Dyke, C. A.; Stewart, M. P.; Tour, J. M. *J. Am. Chem. Soc.* **2005**, *127*, 4497–4509.
(43) Bachilo, S. M.; Strano, M. S.; Kittrell, C.; Hauge, R. H.; Smalley, R. E.; Weisman, R. B. *Science* **2002**, *298*, 2361–2366.
(44) Crochet, J.; Clemens, M.; Hertel, T. *J. Am. Chem. Soc.* **2007**, *129*, 8058–8059.
(45) Alvarez, W. E.; Pompeo, F.; Herrera, J. E.; Balzano, L.; Resasco, D. E. *Chem. Mater.* **2002**, *14*, 1853–1858.

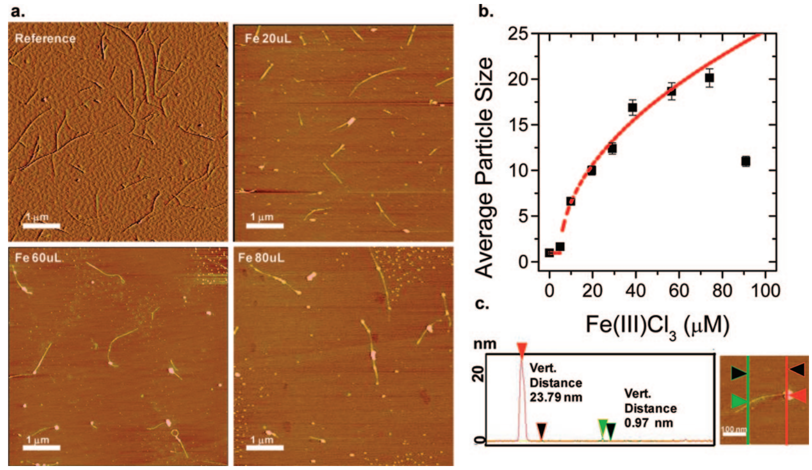

Figure 5. MW electrodeposition kinetics of $FeCl_3$ on SWNT. (a) Representative AFM images of MW induced reduction of Fe^{3+} metal ions. (b) Particle size distribution on the tips of individual SWNTs. (c) Representative AFM image of an individual SWNT–metal complex with their respective vertical distance.

spectroscopic features (Figure 4a–c). The supernatant solution (red trace) is enriched in small-diameter semiconducting SWNTs, while the pellet (orange trace) exhibits an enrichment of metallic tubes. The Raman spectrum of the pellet has a significantly higher baseline, likely attributable to lossy scattering from the gold nanostructures. Interestingly, the G peak from the pellet displays a $-12\ cm^{-1}$ shift, while the intensity of the D band is increased compared to the reference spectrum (Figure 4c). We attribute the D feature to gold nanoparticle attachment, while the G peak shift suggests charge injection from the gold nanoparticles; similar shifts have been reported upon alkali intercalation of SWNT bundles.[46,47] Furthermore, the Breit–Wigner–Fano peak at 1550 cm^{-1} that arises from conduction electrons in metallic SWNT[39] disappears from the semiconductor-enriched supernatant solution, but is prominent in the resuspended pellet, again indicating a strong enrichment in metallic SWNT. Figure 4d is a representative image of the SDBS–SWNT–Au suspension before and after centrifugation; note that the red coloration from gold nanostructures is removed from the centrifuged solution. SWNT bundles comprising both metallic and semiconducting SWNTs[44] are likely activated by the MW process and then removed from solution during centrifugation, accounting for the decreased concentration of semiconducting SWNTs in the final supernatant.

Electrodeposition kinetics were examined in the MW-driven reaction between SWNT–SDBS suspensions and $FeCl_3$, which generates relatively few free-floating particles. Figure 5a shows AFM images of individual SWNTs with metal particle formation with four different initial metal ion concentrations; particles were again predominantly deposited at the ends of the SWNTs. Figure 5b reveals that the size of the metal particles (95% confidence intervals) increases sublinearly with $FeCl_3$ concentrations up to 80 μM. Figure 5c shows a representative AFM image of an individual SWNT with attached nanoparticles at its tips and their respective vertical heights. Initial $FeCl_3$ concentrations above 80 μM yields spontaneous sedimentation of SWNT–metal complexes after MW treatment; this probably accounts for the decrease in observed particle size with the highest iron concentrations. No nanoparticles were detected with starting iron concentrations below 5 μM, which could be attributed to SDBS sequestration of Fe(III) cations at sites inaccessible to reduction by SWNT tips (at SWNT sidewalls or on free SDBS micelles). X-ray photoelectron spectroscopy (XPS) indicated that the particles formed were a mixture of reduced and oxidized iron (see Supporting Information). We note that some or all of the observed oxygen could have been introduced after the initial Fe deposition process. SWNT–Fe suspensions that were not exposed to MW failed to produce any detectable Fe signature by XPS. (X-ray diffraction (XRD) was also performed, but gave no definite result due to the strong background of the surfactant and the low volume fraction of Fe particles).

The kinetics of diffusion-limited electrodeposition on ultramicroelectrodes is well described by[48]

$$I = \left(\frac{zFD^{1/2}c}{\pi^{1/2}t^{1/2}}\right) + \left(\frac{zFDc}{r_o}\right) \quad (1)$$

where I is current density, z is ion valence, F is Faraday's constant, D is the diffusion coefficient of the Fe(III) ions, c is the molar concentration of ions, r_o is the particle radius, and t is time. Neglecting the first term in eq 1 (unimportant for submicrometer diameter electrodes[48]), we can expand the current density term (yielding $q/t = zFDc\pi r_o$, where q is charge and using πr_o^2 for the cross-sectional area), express the amount of deposited material in moles ($M = q/zF$), and assume a spherical deposit (of volume $v = {}^4/_3\pi r_o^3$) expressed as its molar volume V_m to obtain an expression for expected particle size as a function of time, diffusion constant, and initial concentration of acceptor species:

$$r^2 = 0.75V_mDct \quad (2)$$

Equation 2 yields a near-quantitative match to the experimental data using $t = 1$ s, Fe^0 molar volume $V_m = 7.09\ cm^3/mol$, and Fe(III) diffusion rate $D = 3 \times 10^{-6}\ cm^2\ s^{-1}$.[49] This satisfying agreement between experiment and established kinetic theory (Figure 5b, red curve) for electrodeposition at ultramicroelectrodes strongly suggests that formation of iron nanoparticles proceeds at or near diffusion limited rates and implies electrodeposition currents on the order of 10^{-15} A per SWNT tip.

(46) Claye, A.; Rahman, S.; Fischer, J. E.; Sirenko, A.; Sumanasekera, G. U.; Eklund, P. C. *Chem. Phys. Lett.* **2001**, *333*, 16–22.
(47) Claye, A. S.; Nemes, N. M.; Janossy, A.; Fischer, J. E. *Phys. Rev. B* **2000**, *62*, R4845–R4848.
(48) Milchev, A.; Stoychev, D.; Lazarov, V.; Papoutsis, A.; Kokkinidis, G. *J. Cryst. Growth* **2001**, *226*, 138–147.
(49) Bluhm, E. A.; Schroeder, N. C.; Bauer, E.; Fife, J. N.; Chamberlin, R. M.; Abney, K. D.; Young, J. S.; Jarvinen, G. D. *Langmuir* **2000**, *16*, 7056–7060.

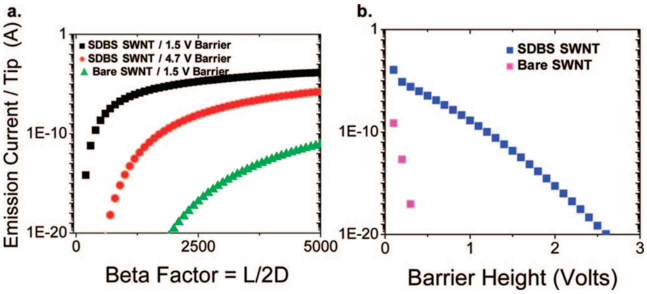

Figure 6. Emission current of SWNTs in MW fields ($\langle E\rangle = 3.45E^5$ V/m) for a SWNT of 1 nm in diameter. (a) Emission current as function of tube length for bare (green) and a surfactant-covered tube with a barrier of 1.5 V (black) and 4.5 V (red). (b) Emission current as function of compression barrier for bare (purple) and SDBS-covered (blue) SWNTs with an average length of 500 nm.

We note that if the iron nanoparticles are oxidized (which increases their molar volume, iron basis), then the deposition rate could be as much as a factor of 2 lower (the molar volumes of FeO, Fe_3O_4, and Fe_2O_3 are 11.97, 14.92, and 15.20 cm^2/mol, respectively). Using the different molar volume values of the oxide Fe in eq 1, we obtained reasonable agreement to our experimental observation (see Supporting Information).

The fundamental mechanism involved in this simple antenna chemistry is an important question to consider. Reactant cations (e.g., $Fe(OH)_2^+$) may associate with the surfactants' sulfonate anions before reduction, while anionic reactants (e.g., $AuCl_4^-$) must reside outside the surfactants' outer Helmholtz plane.[50] Therefore, nanoparticle formation likely involves a long-range electron transfer of at least 3 to 5 nm. A similar process was described by Graetzel,[51] who conclusively demonstrated a long-range tunneling mechanism for redox reactions across self-assembled monolayers of alkane thiols on biased gold electrodes. We estimate that the minimum electron transfer rate needed to generate observable nanoparticles in 10 s to be at least 10^{-18} A (assuming an effective duty cycle of 10%, 100 atoms per particle, and 3 e^- per Fe ion, we can estimate a nanoparticle size of around 1.1 nm^3 or 1.3 nm in diameter, well within the resolution of AFM), while the larger particles seen would require currents in the vicinity of 10^{-16} to 10^{-15} A. Tunneling current through a potential barrier Φ under high electric field βE is described by the Fowler−Nordheim (F-N) equation.[10] We quantitatively explored the origin of these rather substantial electrodeposition currents by systematically varying the sensitive variables Φ, β, and E (computational details are in Supporting Information).

We first consider the case of a bare metallic SWNT immersed in a hydrocarbon dielectric ($k = 2.3$). For analyzing nanotube field emission measurements in vacuo, Φ is normally set to their work function ~4.7 V.[52] That Φ value generates impossibly low currents under our conditions, however. Figure 6a (green trace), shows the expected emission current (per SWNT tip) for SWNTs of various lengths when Φ is set to 1.5 V, the oxidation potential of a 1 nm diameter metallic SWNT. This indicates that only SWNTs of several micrometers in length would generate detectable nanoparticles, which is contrary to our experimental observations—nanoparticles occur commonly on the tips of SWNTs down to a few hundred nanometers in length. Figure 6b shows the tip currents expected from 500 nm long tubes while varying the effective barrier height Φ; this indicates that Φ must be in the 0.25−0.30 V range to generate currents consistent with observations. This range is not impossibly low, but seems unrealistic, even noting that there exist multiple reports of long-range electron transfer reactions at scanning probe (STM) tips wherein effective barriers of less than 1V have been observed.[53−55]

We next consider the more complex case of SWNT coated with a thin insulator in an aqueous environment and develop a simple model explaining the gradient compression visualized in the 'SDBS−SWNT' image in Figure 1a. Compared to the 'bare−SNWT' case, it appears that essentially all of the field gradient around the tip of the nanotubes is compressed into the thin surfactant coating. On the basis of electrostatics and SWNT−surfactant−electrolyte 'electrode' geometry (computational details in Supporting Information), we estimate this compression factor ζ to be ~16 in the case of 1 nm diameter HiPco SWNT with an SDBS surfactant coating (see Supporting Information Figure S8). We note in passing that the hemispherical capacitor formed at the tip of the nanotubes is sufficiently small, ~1.6×10^{-19} F, that adding one electron to the tip of the nanotube will raise its potential by about one volt. Including the gradient compression factor, Figure 6a shows the expected emission current assuming barriers of 4.7 V (red trace) and 1.5 V (black trace). If the tunnel barrier is 4.7 V, then the short tubes (~200 nm long) cannot generate enough current to produce nanoparticles. With a barrier of 1.5 V, however, then the expected emission current is sufficient for short tubes to produce nanoparticles, as observed experimentally. The blue trace in Figure 6b shows emission current for 500 nm long SWNT (1 nm diameter) as a function of barrier height. Interestingly, barriers around 1.7 V produce emission in the 10^{-15} A range, consistent with our experimentally observed deposition rates. Careful additional study is certainly needed, but we consider the experimental results to be consistent with a classic Fowler−Nordheim field emission process through a barrier roughly equal to the SWNT oxidation potential, noting that the apparent field strength is substantially augmented by the nanotubes' geometric factor β as well as the gradient 'compression' factor ζ within the surfactant layer.

Conclusions

We have found compelling evidence for 'antenna chemistry' using highly dispersed SWNT−surfactant suspensions in microwave fields at 2.54 GHz. Electric-field-driven redox processes with reducible transition metal salts result in tip-specific deposition of metallic nanoparticles and sheaths, yielding novel nanoparticle−nanotube structures. We find substantial evidence that metallic nanotubes participate preferentially in these reactions, which suggests a general route for separating and fractionating metallic nanotube species. Reduction of Fe(III) species to produce nanoparticles on the SWNT tips appears to proceed at or near diffusion-limited rates. These redox processes appear to proceed via a long-range electron transfer mechanism involving tunneling or outright field emission into solution. The effective electric field at the tips of metallic SWNT is enhanced by their aspect ratio as well as a gradient 'compression' effect caused by the thin, low-κ dielectric shell of surfactant molecules.

(50) Nozik, A. J. *Annu. Rev. Phys. Chem.* **1978**, *29*, 189–222.
(51) Miller, C.; Cuendet, P.; Gratzel, M. *J. Phys. Chem.* **1991**, *95*, 877–886.
(52) Suzuki, S.; Watanabe, Y.; Homma, Y.; Fukuba, S.; Heun, S.; Locatelli, A. *Appl. Phys. Lett.* **2004**, *85*, 127–129.
(53) Halbritter, J.; Repphun, G.; Vinzelberg, S.; Staikov, G.; Lorenz, W. J. *Electrochim. Acta* **1995**, *40*, 1385–1394.
(54) Kuznetsov, A. M.; Ulstrup, J. *Electrochim. Acta* **2000**, *45*, 2339–2361.
(55) Nagy, G.; Wandlowski, T. *Langmuir* **2003**, *19*, 10271–10280.

Reduction of transition metal salts under these conditions to produce nanoparticles further implies strong rectification despite symmetric AC field stimulation. We anticipate that the novel composite nanostructures produced by this approach could prove to be useful nanoelectronics and catalysts, while the underlying electron transfer and rectifying processes could eventually lead to interesting applications in energy harvesting, nanomedicine, and chemical synthesis.

Experimental Methods

SWNT−microwave (MW) interactions were studied using aqueous surfactant suspensions of individualized raw HiPco SWNT[56] (batch number 164.4) produced in the Carbon Nanotechnology Laboratory at Rice University. The surfactant suspensions were prepared using homogenization, ultrasonication, and ultracentrifugation following standard literature methods.[2] Deionized (DI) water (18 MΩ resistivity) obtained from a NanoPure system (Barnstead, Dubuque, IA) was used throughout this work. Surfactants employed included Pluronics (F88-Prill, BASF), sodium dodecyl sulfate (SDS, 99+%, Aldrich), dodecylbenzenesulfonic acid, sodium salt (SDBS, 99+%, Aldrich), Triton-X (TX-100, 99%, Aldrich), and cetyltrimethyl-ammonium bromide (CTAB, 99%, Aldrich); all were used as received and employed at 1 wt % in DI water. The SWNT concentration in suspensions were adjusted to 10 mg/L; SWNT concentrations were determined by absorbance.[57] Transition metal salts, all used as received from Aldrich, were used as redox agents, including gold ($HAuCl_4$, 99.999%), silver ($AgNO_3$, 99.999%), palladium (K_2PdCl_4, 99.99%), platinum (H_2PtCl_6, 99.995%), copper ($CuCl_2$, 99.999%), tin ($SnCl_2$, 99.99%), and iron ($FeCl_3$, 99.99%). All metal salt solutions were prepared at a concentration of 1 mM in DI water. Unless otherwise stated, all MW reactions were performed in a $MARS_X$ (CEM Corporation, Matthews, NC) operating at 2.54 GHz (multimode) with 1000 W for 10 s. MW reactions were performed with 1 mL of SWNT suspension (plus variable amounts of metal salt solution, as noted) in 2 mL glass vials (1 cm diameter × 3 cm tall). The (uncapped) sample vials were placed over the geometric center of the MW reactor on an inverted Pyrex dish (80 × 40 mm); no other accessories were placed inside the reactor.

Unless otherwise stated, all spectroscopic measurements were obtained with 1 mL of SWNT−surfactant mixture in a sterile 1.5 mL polymethylmethacrylate (PMMA) cuvette (LPS, L324101). UV−visible−NIR absorbance and fluorescence spectra were obtained with a Nanospectralyzer Model NS1, Version 1.95 (Applied Nanofluorescence, Houston, TX). Absorbance spectra were obtained in the visible and near-infrared regions (400−1400 nm) using integration times of 500 ms and 10 accumulations. The SWNT fluorescence was excited at 660 nm, and emission spectra were obtained between 900 and 1400 nm using 500 ms integration times and 10 accumulations. Absorbance at 763 nm was used to normalize the fluorescence spectra. *Liquid-phase* Raman measurements were obtained using 785, 633, and 514 nm laser excitation with an inVia micro-Raman spectrometer (Renishaw, Gloucestershire, U.K.). Liquid samples were held in a Renishaw Raman Macro Sampling Set in a 2 mL glass vial. Raman spectra were collected from 100 to 3200 cm^{-1} with Wire2 data acquisition software, using 20 s exposure times and 1 accumulation.

Atomic force microscope (AFM) images were obtained with a Nanoscope IIIa (Digital Instruments/Veeco Metrology, Inc., Santa Barbara, CA), operating in tapping mode, using 1−10 Ohm-cm phosphorus (*n*) doped Si tips (Veeco, MPP-11100−140) at a scan rate of 2 Hz and 512 × 512 resolution. Samples for AFM analysis were prepared with 20 μL of SWNT suspensions spin coated at 3000 RPM onto roughly 0.25 cm^2 freshly cleaved mica surfaces (Ted Pella, Inc., Redding, CA) and rinsed with DI water and 2-isopropanol to remove the excess of surfactant. Samples were left spinning for 10 min to dry thoroughly.

X-ray photoelectron spectroscopy (XPS) was performed on a PHI Quantera SXM scanning X-ray microprobe (Chanhassen, MN) with a pass energy of 26.00 eV, 45° takeoff angle, and a 100 μm beam size. The samples were collected after inducing flocculation of the SWNT−Fe suspension via acetone addition.

X-ray diffraction (XRD) was performed on a Rigaku SmartLab X-ray Diffractometer with a Cu X-ray tube. The samples were prepared on a glass slide by 15 subsequent additions of 10 μL of the solution and letting it dry at room temperature to obtain a uniform layer of the sample.

Acknowledgment. The authors thankfully acknowledge financial support from the Robert A. Welch Foundation (C-1668), and the NSF Center for Biological and Environmental Nanotechnology (EEC-0118007 and EEC-0647452), helpful discussions with James M. Tour and Robert Hauge, and experimental assistance by Alex Eukel.

Supporting Information Available: Particle size distribution histogram, *liquid-phase* Raman spectra with 785, 633, and 514 nm excitation wavelength, fluorescence spectrum (660 nm excitation wavelength) of semiconducting SWNT with different transition metal salts, procedure to generate electric field structure around metallic SWNT using COMSOL Multiphysics 3.4 software, derivation of SWNT redox landscape chart, effective electric field strength calculations, and metallic SWNT alignment calculations. This material is available free of charge via the Internet at http://pubs.acs.org.

JA803300U

(56) Carver, R. L.; Peng, H. Q.; Sadana, A. K.; Nikolaev, P.; Arepalli, S.; Scott, C. D.; Billups, W. E.; Hauge, R. H.; Smalley, R. E. *J. Nanosci. Nanotechnol.* **2005**, *5*, 1035–1040.

(57) Attal, S.; Thiruvengadathan, R.; Regev, O. *Anal. Chem.* **2006**, *78*, 8098–8104.